Revision 1

Correction 20140714

Near-infrared investigation of folding sepiolite

Maria Tsampodimou, Vanessa-Jane Bukas*, Elizabeth T. Stathopoulou†, Vassilis Gionis, and Georgios D. Chryssikos

Theoretical and Physical Chemistry Institute, National Hellenic Research Foundation, 48 Vass. Constantinou Ave., Athens, Greece 11635.

Present Address:

* Department of Theoretical Chemistry, Technische Universität München, Lichtenbergstr. 4, Garching 85747, Germany.

† Department of Historical Geology and Palaeontology, Subfaculty of Geology & Geoenvironment, University of Athens, Panepistimiopolis, 15784, Zografou, Athens, Greece.

Abstract

Sepiolite is an industrially important clay mineral of the palygorskite-sepiolite group with alternating 2:1 ribbons and hydrated tunnels. Dry sepiolite, $Mg_8Si_{12}O_{30}(OH)_4(OH_2)_4$, looses half of its OH_2 content upon further heating and undergoes a structural collapse known as folding. This treatment is considered essential for enhancing the absorptive properties of the clay. In this paper, the folding process is studied by near-infrared (NIR) spectroscopy, mid-infrared attenuated total reflectance (ATR) and thermogravimetric analysis (TGA). The folded state, $Mg_8Si_{12}O_{30}(OH)_4(OH_2)_2$, reveals a new spectrum of fundamental and higher-order OH_2 vibrations, as well as systematically split doublets of structural and surface O-H vibrations. Detailed assignments for the stretching, combination and overtone O-H modes are proposed on the basis of the two non-degenerate populations of Mg_3OH (and SiOH) present in the folded state. It is demonstrated that NIR is of particular diagnostic value in monitoring conveniently and non-invasively the folding process, which appears as a simple transition between well-defined dry- and folded-structures. At the level of elementary sepiolite particles (laths), folding is described as a cooperative process requiring the integrity of the ribbons and the inter-ribbon linkages (moderately acid-leached sepiolite does not fold). This is opposed to the skewed and sometimes complex OH_2 desorption trace observed by high-resolution TGA, which appears to indicate a multimodal distribution of laths. It is proposed that the rate-determining step for a sepiolite (also, palygorskite) lath to fold is the creation of a critical zone at mid particle length which is OH_2-deficient and contains unstable, fivefold-coordinated Mg^{2+}.

Keywords: sepiolite, palygorskite, folding, acid activation, near-infrared spectroscopy, ATR, high-resolution TGA

Introduction

Sepiolite is a member of the palygorskite-sepiolite group of clay minerals with main industrial applications as rheology modifier and absorbent, but also as carrier, catalyst support etc. (Galan 1996; Álvarez et al. 2011). It is a trioctahedral phyllosilicate with ideal formula $Mg_8Si_{12}O_{30}(OH)_4(OH_2)_4{\cdot}zH_2O$ per half unit cell ($z\approx8$ at ambient), a modulated structure and a lath-like particle morphology (Brauner and Preisinger 1956; Post et al. 2007). Modulation is manifested by the periodic reversal of the apical Si-O bonds in the tetrahedral sheet every three pyroxene chains and the concomitant discontinuity of the octahedral sheet (Fig. 1a). As a result, sepiolite consists of alternating 3-chain, trioctahedral 2:1 ribbons and hydrated tunnels. The term "tunnel" is preferred here over the more commonly used term "channel" because the latter is reserved to describe the grooves (i.e. open "tunnels") running along the external surface of the particles. Two types of tunnel H_2O are shown in the formula: two coordinated OH_2 per "exposed" Mg^{2+} cation on the edges of the discontinuous octahedral sheet and "zeolitic" (z) H_2O filling the tunnels. In addition to these types, there is also H_2O on the external surface of the particles, interacting with the abundant silanol (SiOH) terminations of the tetrahedral sheet, and physisorbed H_2O. All H_2O except the Mg-coordinated OH_2 species desorb below ~130-150 $^{\circ}$C (Nagata 1974; Frost and Ding 2003),

leaving the structure open (Post et al. 2007) and the inner surface of the tunnels exposed (Ruiz-Hitzky 2001).

Heating palygorskite-sepiolite clays at higher temperatures (~300 °C) induces the removal of one OH_2 per Mg, causes the folding of the structure (Fig. 1b) and results in the collapse of the tunnels (Preisinger 1963; Post et al. 2007). This folding event is of technological importance ("calcination") because it marks the loss of microporosity and colloidal properties of the clays, and leads to the enhancement ("activation") of mesoporous absorptive properties, such as oil bleaching performance (McCarter et al. 1950; Haden and Schwint 1967; Álvarez et al. 2011).

Hayashi et al. (1969) were the first to study systematically the high temperature transformations of sepiolite by mid-infrared spectroscopy and XRD. In the temperature range of folding, they found that the single Mg_3O-H stretching band of sepiolite splits into two components due to the simultaneous presence of folded and unfolded structures. Subsequent thorough mid-infrared studies by Serna et al. (1975) and Prost (1975) confirm the observations of Hayashi et al. (1969) regarding band splitting, but assign the appearance of the two OH stretching components to the rearrangement of H-bonding patterns in sepiolite induced by folding. The near-infrared (NIR) spectra of sepiolite subjected to folding by calcination have been recently reported by Mora et al. (2010) but their analysis is contrary to the previous literature because it assumes the coexistence of trioctahedral and dioctahedral layers.

The present paper reports on the NIR spectrum of folded sepiolite, extending a recent study of drying sepiolite (Bukas et al. 2013) to higher temperatures. The structural OH and H_2O overtone and combination fingerprints of the folded structure are assigned on

the basis of the fundamental modes observed in the mid- infrared by Attenuated Total Reflectance (ATR). Folding is recognized as a cooperative structural transformation which takes place abruptly during the course of OH_2 desorption.

Materials and Methods

This study is based on sepiolite SepSp-1 (Valdemore, Spain), obtained from the Clay Minerals Society repository and ground to less than 250 μm. Supplementary measurements were performed on a second sepiolite sample (CAB), collected from the Cabañas de la Sagra mine during the field trip of the 2010 Trilateral Meeting on Clays (Seville, Spain). Acid treatment of SepSp-1 was performed in 2M H_2SO_4 for 1 h, followed by thorough rinsing and drying at ambient. Portions (~500 mg) of the pristine and acid-treated samples, placed in colorless borosilicate flat-bottom vials, were subjected to thermal treatments in an electrical furnace at ambient pressure and temperatures ranging from 150 to 550 $^{\circ}$C at a step of 12±1 $^{\circ}$C. Residence time at each temperature was 1 h. Immediately after the completion of each heating step, the vial was sealed, left to cool to ambient and measured by infrared spectroscopy. Subsequently, it was opened and re-introduced to the furnace at the next higher temperature.

NIR spectra (3800-8000 cm^{-1}) were collected on a Fourier-transform instrument (Vector 22 by Bruker Optics) equipped with an integrated sphere accessory. Each spectrum represents the average of 200 scans at a resolution of 4 cm^{-1}. Selected samples in the folded state were measured in the mid-infrared (550-4000 cm^{-1}) by a single reflection diamond ATR accessory (Durasampl IR II by SensIR) on a Fourier transform spectrometer (Equinox 55 by Bruker Optics) under N_2-purge. The ATR spectra represent

the averages of 50 scans at a resolution of 2 cm^{-1}. Peak maxima were resolved by 2nd derivative analysis using the Savitzky-Golay algorithm of the OPUS software, as in Bukas et al. (2013).

Thermogravimetric (TGA) data were collected on a Q500 TA Instruments analyzer. Measurements were performed on 12-15 mg samples placed in Pt pans under a flow of very pure N_2 gas ($H_2O \leq$ 5 ppm, 60 and 40 ml/min in the sample and balance areas, respectively). Constant heating rate experiments were performed (q=0.5-20 $^{\circ}$C/min) and complemented with dynamic heating rate measurements (HiRes ^{TM} option) over selected temperature ranges.

Results and discussion

Infrared spectra of folded sepiolite

The ambient infrared spectra of sepiolite subjected to heating at 375 $^{\circ}$C are compared to those of the same sample dried at 175 $^{\circ}$C (Fig. 2). The latter are identical to those reported by Bukas et al. (2013) and represent the ("zeolitically dry") state from which nearly all surface and zeolitic H_2O are removed. Sepiolite heated to 375 $^{\circ}$C is folded (Post et al. 2007). The spectra indicate that folding is associated with major spectral changes over all wavenumber ranges of interest. Most of these changes involve sharp spectral features. These are more conveniently observed in the 2nd derivative spectra (Fig. 3) and summarized in Table I.

The 3680 cm^{-1} Mg_3O-H stretching mode of the zeolitically dry sample splits in two components observed at 3692 and 3674 cm^{-1} (Fig.2). These component bands give rise to a well-defined overtone doublet at 7218 and 7181 cm^{-1} (anharmonicity X=83-84 cm^{-1})

and couple with a bending mode δ at 657 cm^{-1} to produce a (ν+δ) combination doublet at 4327, 4310 cm^{-1} (Fig. 2 and 3).

The vibrational signature of H_2O in the folded state is also evident: Two sharp H_2O stretching fundamentals at 3601 and 3532 cm^{-1} are observed in the ATR spectra with overtones at 6980, 6915 cm^{-1} (X=111, 75 cm^{-1}) in the NIR. The H_2O stretching fundamentals combine with a single bending mode at 1613 cm^{-1} to produce a sharp (ν+δ) combination doublet at 5191 and 5122 cm^{-1} (X=23 cm^{-1}) as well as a weaker (ν+2δ) doublet at 6750 and 6690 cm^{-1} (Fig. 2).

Surface SiOH groups in folded sepiolite, produce a characteristic triplet higher-order signature (7307, 7283, 7264 cm^{-1}, Fig. 2 and 3) instead of the single ~7270 cm^{-1} mode of dry sepiolite. The two higher-energy components at 7307 and 7283 cm^{-1} are extremely sensitive to moisture and disappear quickly upon exposure to ambient atmosphere, whereas the 7264 cm^{-1} band is less sensitive to rehydration. Indeed, partial rehydration may explain why only one SiO-H stretching fundamental is observed by ATR spectroscopy at approx. 3719 cm^{-1} (Fig. 2) whereas the corresponding NIR spectra of sealed samples reveal at their low frequency end discrete SiO-H fundamentals at 3717, 3725 and 3740 cm^{-1} (Fig. 3, Table 1). Silanol stretching-bending combinations are observed at 4569 and 4544 cm^{-1} (Fig. 3). These combination modes invoke the involvement of a relevant fundamental above ~855 cm^{-1}, perhaps the peak observed at 864 cm^{-1} (Fig. 3).

Finally, the ATR spectrum of the 375 °C sepiolite reveals a signature of Si-O fundamental modes in the 1200-900 cm^{-1} range, which is significantly more complex that the

157 corresponding profile of the 175 °C sample. The highest frequency component of this
158 envelope which is attributed to the Si-O-Si bonds linking adjacent ribbons is observed at
159 ~1150 cm^{-1}, i.e. at energies lower than those of the dry and ambient states (1195, 1212
160 cm^{-1}, respectively; Bukas et al. 2013).

161 Based on the above, the overall vibrational signature of sepiolite heated to 375 °C cannot
162 be reconciled with that of a mixture of folded and unfolded material (Hayashi et al.
163 1969). Instead, the structural features of folded sepiolite, which are known from XRD
164 (Brauner and Preisinger 1956; Post et al. 2007), are sufficient in providing a satisfactory
165 spectral interpretation: Upon folding, the parallelogram cross-section of the tunnels
166 ceases to be orthogonal (Fig. 1b). As a result, the two structural Mg_3OH species lining
167 the side of each ribbon are no longer identical: one is in the acute angle of the
168 parallelogram and the other in the obtuse one. In Post et al. (2007) these species are
169 labeled OH-2 and OH-2b, respectively. The presence of two distinct Mg_3OH species can
170 explain why the Mg_3O-H modes of the folded state appear as doublets of approximately
171 equal intensity at 3692, 3674 cm^{-1} (stretching fundamentals), 4327, 4310 cm^{-1}
172 (combinations) and 7218, 7181 cm^{-1} (overtones). It has been suggested (Serna et al.
173 1975) that the high energy component of the fundamental stretching doublet (3692 cm^{-1})
174 may correspond to the OH-2 species (acute angle) being perturbed by the remaining Mg-
175 coordinated OH_2 species via repulsive H···H interactions. However, the O···O distance
176 between these OH and OH_2 species is about 4.8 Å (Post et al. 2007) and is therefore
177 unlikely to cause a significant blue-shift of the OH-2 stretching. Instead, the deformation
178 of the ribbon itself which is induced by folding is anticipated to play a bigger role in
179 differentiating between the energy of the OH-2 and OH-2b modes. For example,

according to the refinement by Post et al. (2007), the three Mg-O bonds of the Mg_3OH-2 species inside the acute angle of the folded tunnel average 2.04 Å in length, whereas those of its OH-2b counterpart in the obtuse angle average 2.06 Å. Other factors assumed constant, the shorter average Mg-O length would imply a longer O-H and a lower stretching frequency in OH-2 compared to OH-2b. Based on this analysis and contrary to the suggestion of Serna et al. (1975) the high energy stretching, combination and overtone components at 3692, 4327, 7218 cm^{-1} are attributed to Mg_3OH-2b (obtuse angle) and their lower energy counterparts at 3674, 4310 and 7181 cm^{-1} to Mg_3OH-2 (acute angle).

Similarly, folding splits the degeneracy of the SiOH groups, as remarked first by Serna et al. (1975): One subset of SiOH groups point towards the adjacent ribbon, establish H-bonds with the siloxane sheet and is expected to rehydrate slowly at ambient. The other subset point away from the ribbons and remain vulnerable to rehydration upon exposure to ambient humidity.

NIR monitoring of the folding process

The structural changes occurring in the range of folding are conveniently studied by monitoring the OH stretching overtones and H_2O combination modes as a function of temperature (Fig. 4). The low-temperature (<150 $^{\circ}C$) part of the bubble graphs corresponds to the zeolitic dehydration event, reported and discussed in detail by Bukas et al. (2013). The occurrence of folding can be identified as a sharp transition at 275±5 $^{\circ}C$ by the aforementioned splitting of the 7192 cm^{-1} Mg_3OH overtone, or the appearance of the sharp 5191 cm^{-1} H_2O combination mode. Repeating the experiment with higher

residence times at each temperature or with smaller amounts of sample does not shift the temperature of the transition and does not affect its spectroscopic signature, suggesting the absence of kinetic effects. Beyond this transition and up to ~450 °C all spectral features remain remarkably constant in position, width and relative intensity. Above ~450 °C all bands begin to fade out, marking the onset of higher temperature events which are beyond the scope of this paper.

Clearly, within the temperature resolution of this experiment, folding is an abrupt, well defined structural transformation taking place over a temperature range of less than 15 °C (Fig. 4). Sepiolite CAB displays exactly the same NIR patterns as SepSp-1 (not shown) but a slightly lower folding temperature (250±5 °C).

Interestingly, early signs of the folding can be observed mainly in the region of SiOH overtones, approximately 50 °C below the previously defined folding transition. In SepSp-1, the characteristic 7270 cm^{-1} SiO-H stretching overtone begins to weaken at ~225 °C, shift towards 7264 cm^{-1} and produce two new bands at 7283 and 7307 cm^{-1} (Fig. 4). A similar early sign of folding is manifested as a shift of the weak ~5270 cm^{-1} H_2O combination band. We propose that these early changes are due to the dehydration of the external surface of sepiolite which is modifying the vibrations of the surface SiOH groups. More specifically, the Mg^{2+} cations terminating the exposed ribbons on the surface of the elementary particles need to complete their 6-fold coordination with OH_2 species in a manner similar to their "bulk" counterparts. But unlike coordinated OH_2 in the tunnels, these channel OH_2 species interact with SiOH groups and physisorbed H_2O at ambient conditions, or solely with SiOH above ~100 °C. As a result of this difference, channel OH_2 species are assumed to desorb at lower temperatures than tunnel OH_2

226 leading to the bonding reorganization of the SiOH group before the actual folding of the
227 tunnels. This interpretation is compatible with the observation that the silanol spectrum
228 (hence, also, the 6-fold coordination of the outer surface Mg) recovers quickly upon
229 exposing the folded sample to ambient humidity, whereas the structure remains folded.
230

231 **Thermogravimetric analysis in the range of folding**

232 The derivative thermogravimetric (DTG) data of Fig. 5 show the three dehydration events
233 of SepSp-1 and CAB up to 700 °C (surface/zeolitic <120 °C, 1st OH_2 at 150-325 °C and 2nd
234 OH_2 at 400-700 °C) in agreement with earlier studies (e.g. Frost and Ding 2003). The
235 apparent activation energies, E_a, of these processes can be calculated from the
236 temperature shift of the DTG maxima, T_{max}, according to the method of Kissinger (1957).
237 Thus, the zeolitic, first and second OH_2 dehydration events of SepSp-1 are assigned
238 values of E_a =85±10, 100±10 and 210±10 kJ/mol, respectively. Very similar values (85,
239 115 and 210 kJ/mol, respectively) were determined for sepiolite CAB. Activation
240 energies for the last two dehydration events have been determined previously by the same
241 methodology on sepiolites from Japan and Turkey (Kiyohiro and Otsuka 1989) and
242 compare favorably with those reported here.
243 A comparison of the characteristic folding temperatures of sepiolite determined
244 independently by thermogravimetric and structural techniques is not straightforward, as
245 the heating rate is by no means the main determinant. For example, the NIR
246 spectroscopic monitoring experiment of SepSp-1 (Fig. 4) corresponds to q≈0.2 °C/min
247 and displays the switching to the folded state at 275 °C, which is ~50 °C higher than the
248 corresponding dehydration event of the same sample measured at similar q by TGA (Fig.

249 5). In addition, the synchrotron XRD monitoring experiment of Post et al. (2007), which
250 was performed in air at a rate of ~5 °C/min, reports the folding of a sepiolite from
251 Durango, Mexico, at even higher temperature (~325 °C). Duplicate SepSp-1 samples
252 were measured by TGA either at q=0.2 °C/min or by the step-wise heating program
253 employed in the NIR experiment up to 225 °C. These samples were measured
254 subsequently by NIR and found fully folded.
255 These apparent discrepancies in the experimentally determined folding temperatures are
256 attributed to the extreme sensitivity of folding on both the water vapor content and the
257 flow rate of the carrier gas in agreement with Kiyohiro and Otsuka, (1989). Indeed,
258 folding temperatures of sepiolite under vacuum can be as low as 150 °C (Giustetto et al.
259 2011). In this respect, the use of NIR spectroscopy in determining folding in a non-
260 invasive manner and in variable environments is particularly appealing.
261 The pronounced dependence of folding on the experimental dehydration conditions
262 masks subtler effects such as those anticipated by the compositional (García-Romero and
263 Suárez 2010), structural (Sánchez del Rio et al. 2011) or textural (García-Romero and
264 Suárez, 2013) variability of sepiolite, especially when comparing folding evidence from
265 different laboratories or techniques.
266 Interestingly, the shape of the first OH_2 DTG peak of SepSp-1 (Fig. 5) suggests that this
267 peak is a convolution of at least two events, which are not sufficiently resolved even at
268 the slowest practical constant heating rate experiments, e.g. q=0.5 °C/min. Dynamic rate
269 experiments (Hi-Res™, q_o=10 °C/min, resolution =8) have a measured effective heating
270 rate of ~0.2 °C/min over the temperature range of the folding dehydration event and result
271 in better, though not complete, separation (Fig. 6). The high resolution DTG data of

SepSp-1 and CAB suggest that sepiolite folding can have a complex DTG signature, which is poorly understood and rarely discussed.

Effect of acid leaching

Treatment with mineral acids ("acid activation") has been known to enhance the sorption properties of sepiolite (and palygorskite) clays by altering their structure and increasing their surface area (Aznar et al. 1996; Myriam et al. 1998). Numerous studies (e.g. Abdul-Latif and Weaver 1969; Vincente Rodriguez et al. 1995) confirm that acid activation is due to leaching the Mg^{2+} cations from the octahedral sheet of sepiolite. At high concentrations of acid and long times of treatment, leaching becomes quantitative and leads to the formation of high-surface area fibrous silica (Myriam et al. 1998). However, if the leached fraction of Mg^{2+} is kept below approx. 33% the structure of sepiolite retains its integrity (Esteban-Cubillo et al. 2008).

The NIR spectra of SepSp-1 subjected first to acid leaching (2M H_2SO_4 for 1h) and then to heating at 175 or 375 $^{\circ}$C (Fig. 7) are compared to those of non-leached sepiolite (Fig. 2). The 175 $^{\circ}$C spectra are little affected by acid. All the sharp features related to the octahedral sheet or the OH_2 species suffer a ~40% decrease in intensity but persist leaching. It is therefore concluded that the employed leaching conditions preserve the structural integrity of sepiolite. An important difference between the 175 $^{\circ}$C untreated and leached samples is observed in the spectral regions of SiO-H combination and overtone activity. The sharp bands of the untreated sample gain in intensity and broaden upon leaching (Figs. 2 and 7). The combination mode at ~4570 cm^{-1} does not shift, but the stretching overtone at 7270 cm^{-1} nearly vanishes and gives its place to a strong band

295 at ~7320 cm^{-1} (fundamental at 3742 cm^{-1}, anharmonicity X=82 cm^{-1}, mid-infrared data not
296 shown). The new bands are similar to those of hydrated silica (Morrow and McFarlan
297 1992; Carteret 2009) and constitute the signature of the SiOH groups in the Mg^{2+}-
298 depleted, silica-like portion of the leached sepiolite. Very similar spectra have been
299 reported for smectites subjected to acid treatment (Madejová et al. 2009).
300 Remarkably, the spectrum of the acid leached sepiolite subjected to heating at 375 °C
301 (Fig. 7) is almost identical to that of the same sample heated at 175 °C and does not
302 exhibit the characteristic doubling of Mg_3OH modes which was associated previously
303 with folding (Fig. 2). The full spectral evolution of the acid treated structure on
304 temperature is shown in Fig. 8 and can be compared to that of untreated sepiolite (Fig. 4).
305 Acid treated sepiolite SepSp-1 does not fold at 275 °C. Instead, the spectra remain almost
306 intact up to 375 °C and then progressively fade out without signs of folding. This
307 observation confirms Valentin at al. (2007): Leaching a critical fraction of the octahedral
308 sheet may preserve the modulated structure but breaks the connectivity which is
309 necessary for folding to take place. Folding is a cooperative process.
310
311 **Structural considerations of cooperative folding.**
312 As shown by Post et al. (2007), the ribbons of the folded structure are locked in place not
313 only by OH_2 …O interactions but also by means of weak inter-ribbon Mg-O bonds (2.77
314 Å long), one per edge Mg^{2+} ion (Fig. 1b). These bonds compensate for the loss of one
315 OH_2 per edge Mg^{2+} and restore in part its 6-fold coordination. Further, the folded state is
316 stabilized by the relaxation of the Si-O-Si inter-ribbon angles which, in the unfolded
317 state, were in a rather unusual 180° configuration. Hence, the folded and unfolded

318 structures are well-defined states and not the end-members of a continuous series of
319 structures which are progressively tilted as the OH_2 content decreases. This conclusion
320 is supported by the constancy of the sepiolite spectra over broad temperature ranges
321 below and above the folding transition, as well as by the sharpness of the transition itself
322 (Fig. 4a).
323 The elementary crystals of sepiolite are lath-like (García-Romero and Suárez 2013). The
324 width of typical laths is ~20-30 nm, suggesting that their cross-section is ~10 unit cells in
325 *ab* or less. Their length along *c* is 1-3 orders of magnitude longer than their width. In the
326 range of the folding transition, a lath elementary crystal of sepiolite is either folded or
327 unfolded. The switching of a single dry lath to the folded state is presumably too fast to
328 be observed by conventional techniques. Nevertheless, one can work out important
329 aspects of the folding mechanism.
330 Folding results in the removal of one OH_2 per edge Mg^{2+}. In its very early stages, the
331 desorption of OH_2 must create on the side of the unfolded tunnel a highly active, fivefold
332 coordinated Mg^{2+} (Fig. 9). One such elementary desorption process alone is not
333 sufficient to induce folding because all neighbouring tunnel-cells remain hydrated and
334 unfolded. Instead, a critical number of elementary OH_2 desorption processes must take
335 place for the lath to fold. More importantly, the fivefold coordinated Mg^{2+} sites produced
336 by the elementary desorption of OH_2 species should not be distributed randomly along *c*
337 or across the *ab* plane of the lath cross-section. Clearly, a critical zone of OH_2-deficient
338 Mg^{2+} in fivefold coordination across *ab* and along *c* is required in order to enable,
339 "nucleate", the folding of a single lath. What mechanisms of OH_2 desorption can lead to
340 the creation of this critical volume?

Let us assume that the desorbing OH_2 species can exit the elementary crystal only from the open tunnel ends and not by diffusing through the wall of the tunnels. This assumption implies that the first, OH_2-deficient, active Mg^{2+} sites will be formed close to the ends of the tunnel, which may explain the pronounced dependence of folding on the partial pressure of H_2O in the surrounding environment. Once formed, the active fivefold coordinated Mg^{2+} cations can serve as temporary sites for other OH_2 species hopping out from deeper inside each tunnel. Eventually, this simple model leads to extended OH_2-deficiency over a segment at mid-length of the tunnel. Further, as all tunnels of an elementary crystal are of equal length, a foldable OH_2-depleted zone will be created at mid-length of the lath. When this zone reaches a critical length (hence, volume), it will collapse and induce the folding of the elementary particle. This tentative description is the one-dimensional analogue to the model of Ferrage et al. (2007). These authors described the dehydration of montmorillonite as involving a local layer collapse and a concomitant forced-diffusion of desorbing H_2O propagating in two-dimensions.

The as-described folding of elementary sepiolite crystals is a simple cooperative collapse process. As such, it cannot account for the complexity which is observed in high resolution TGA experiments (Fig. 6). We therefore suppose that the complexity of the DTG traces of folding must be due to the multimodal distribution of laths in the sample. The origins of such distribution may be related to particle size (intrinsic or induced by sample preparation) or compositional effects. For example, the presence of vacancies in the octahedral sheet may affect the stiffness of the ribbon and lower the temperature of folding. This would be in accordance with the observation that dioctahedral palygorskite folds at lower temperatures than trioctahedral sepiolite (Frost and Ding 2003; Post and

Heaney 2008), despite the smaller width of its tunnels which does not seem to impede the OH_2 desorption. By analogy, any type of structure involving sepiolite and/or palygorskite polysomes of different composition or octahedral character (Gionis et al. 2007; Chryssikos et al. 2009; García-Romero and Suárez 2010; Stathopoulou et al. 2011; Suárez and García-Romero 2013) is expected to contribute to the complexity of the folding process.

Implications

In the broader context of relating the rich compositional profile of clay minerals to some of their macroscopic properties, this work comes to demonstrate the robustness of NIR spectroscopy as a tool for monitoring structural rearrangements controllably induced by external perturbations. NIR is employed as a vibrational spectroscopic tool specific to the X-H bond (O-H, but also C-H and N-H). Its non-invasive character, high resolution, accuracy and reproducibility render NIR an efficient indicator when it comes to unmasking subtle effects at the microscopic chemical level due to e.g. compositional variability, a sensitive dependence on environmental conditions, adsoption phenomena, or chemical modification. Further, its flexibility can be transferred smoothly from laboratory to ex situ, high through-put, applications, remotely or via optically transparent media, in industry or in field research, including extra-terrestrial.

In view of the insights regarding the nature of folding in sepiolite, we draw attention to the fact that NIR is efficiently used in probing both, the local elementary chemical process (in this case, the thermal desorption of OH_2 species) and the resulting cooperative

386 macroscopic phase change (e.g. folding). This can be of broader value in the study of
387 other hydrated or hybrid systems undergoing phase changes of cooperative nature.

388 In the particular case of sepiolite-palygorskite minerals, the study of folding can shed
389 light on their possible polysomatism (Stathopoulou et al. 2011; Suárez and García-
390 Romero 2013). In case of particles consisting of both sepiolite or palygorskite ribbons,
391 the critical temperature of cooperative folding will be depending not only on the local
392 structure, which is not expected to differ from that of mixtures, but also on the relative
393 presence of ribbon polysomes and their arrangement (random or segregated) in the
394 elementary particle. In anticipation of an effect of long range order on cooperativity, this
395 study calls for future investigations of sepiolite and palygorskite minerals focusing on the
396 effect of octahedral composition, particle size, morphology and distribution of different
397 types of particles on folding transition temperatures.

398 Last, advances in fundamental materials science and applications may be sought by
399 focusing on the physical treatments or chemical modifications that could lead to and be
400 detected from the loss of cooperative structural changes. Two such cases have been
401 identified in the case of acid-leaching (Valentin et al. 2007) and the pillaring effect in
402 Maya blue-type hybrids (Ovarlez et al. 2009; Tsiantos et al. 2012) but more can be found
403 among the numerous functional materials based on clays and organics (*e.g.* Suzuki et al.
404 2012; Ruiz-Hitzky *et al.* 2013).
405
406
407 **Acknowledgments**

Funding of this work has been provided by Geohellas S.A., the project POLYNANO-KRIPIS 447963/GSRT-Greece and the Applied Spectroscopy Laboratory of TPCI-NHRF. Helpful discussions with George Kacandes of Geohellas S.A. are gratefully acknowledged. MT thanks C. Raptis (Natl. Technical University of Athens) for encouragement and support.

References

Abdul-Latif, N., and Weaver, C.E. (1969) Kinetics of acid-dissolution of palygorskite (attapulgite) and sepiolite. Clays and Clay Minerals, 17, 169-178.

Álvarez, A., Santarén, J., Esteban-Cubillo, A., and Aparicio, P. (2011) Current industrial applications of palygorskite and sepiolite. In E. Galán, A. Singer (Eds.) Development in Clay Science, Vol. 3, Chap. 12, Elsevier, Amsterdam, 2011, pp. 281-298.

Aznar, A.J., Gutiérrez, E., Díaz, P., Alvarez, A., and Poncelet, G. (1996) Silica from sepiolite: Preparation, textural properties and use as support to catalysts. Microporous Materials, 6, 105-114.

Brauner, K., and Preisinger, A. (1956) Struktur und Entstehung des Sepioliths. Tschermaks Mineralogische und Petrographische Mitteilungen, 6, 120-140.

Bukas, V.J., Tsampodimou, M., Gionis, V., and Chryssikos, G.D. (2013) Synchronous ATR infrared and NIR-spectroscopy investigation of sepiolite upon drying. Vibrational Spectroscopy, 68, 51-60.

Carteret, C. (2009) Mid- and near-infrared study of hydroxyl groups at a silica surface: H-bond effect. Journal of Physical Chemistry, 113, 13300-13308.

Chryssikos, G.D., Gionis, V., Kacandes, G.H., Stathopoulou, E.T., Suárez, M., García-Romero, E., and Sánchez del Río, M. (2009) Octahedral cation distribution in palygorskite. American Mineralogist, 94, 200-203.

Estaban-Cubillo, A., Pina-Zapardiel, R., Moya, J.S., Barba, M.F., and Pecharromán, C. (2008) The role of magnesium on the stability of crystalline sepiolite structure. Journal of the European Ceramic Society, 28, 1763-1768.

Ferrage, E., Kirk, C.A., Cressey, G., and Cuadros, J. (2007) Dehydration of Ca-montmorillonite at the crystal scale. Part 2. Mechanisms and kinetics. American Mineralogist, 92, 1007-1017.

Frost, R.L., and Ding, Z. (2003) Controlled thermal analysis and differential scanning calorimetry of sepiolites and palygorskites, Thermochimica Acta, 397, 119-128.

Galan, E. (1996) Properties and applications of palygorskite-sepiolite clays. Clay Minerals, 31, 443-453.

García-Romero, E., and Suárez, M. (2010) On the chemical composition of sepiolite and palygorskite, Clays and Clay Minerals, 58, 1–20.

García-Romero, E., and Suárez, M. (2013) Sepiolite – palygorskite: Textural study and genetic considerations, Applied Clay Science, 86, 129-144.

Gionis, V., Kacandes, G.H., Kastritis, I.D., and Chryssikos, G.D. (2007) Combined near-infrared and X-ray diffraction investigation of the octahedral sheet composition of palygorskite. Clays and Clay Minerals, 55, 543-553.

Giustetto, R., Seenivasan, K., Bonino, F., Ricchiardi, G., Bordiga, S., Chierotti, M.R., and Gobetto, R. (2011) Host/guest interactions in a sepiolite-based Maya blue Pigment: A spectroscopic study. Journal of Physical Chemistry, 115, 16764-16776.

Haden, E.L., and Schwint, I.A. (1967) Attapulgite, its properties and applications. Industrial & Engineering Chemistry, 59, 58-69.

Hayashi, H., Otsuka, R., and Imai, N. (1969) Infrared study of palygorskite and sepiolite on heating. American Mineralogist, 53, 1613-1624.

Kissinger, H.E. (1957) Reaction kinetics in differential thermal analysis, Analytical Chemistry, 29, 1702–1706.

Kiyohiro, T., and Otsuka, R. (1989) Dehydration mechanism of bound water in sepiolite, Thermochimica Acta, 147, 127-138.

Madejová, J., Pentrák, M., Pálková, H., and Komadel, P. (2009) Near-infrared spectroscopy: A powerful tool in studies of acid-treated clay minerals, Vibrational Spectroscopy, 49, 211-218.

Myriam, M., Suárez, M.,and Martín-Pozas, J.M. (1998) Structural and textural modifications of palygorskite and sepiolite under acid treatment, Clays and Clay Minerals, 46, 225-231.

McCarter, W.S.W., Krieger, K.A., and Heinemann, H. (1950) Thermal activation of Attapulgus clay. Industrial & Engineering Chemistry, 42, 529-533.

Mora, M., López, M.I., Ángeles Carmona, M., Jiménez-Sanchidrián, C., and Ruiz, J.R. (2010) Study of the thermal decomposition of a sepiolite by mid-and near-infrared spectroscopies. Polyhedron, 29, 3046-3051.

Morrow, B.A., and McFarlan, A.J. (1992) Surface vibrational modes of silanol groups on silica. Journal of Physical Chemistry, 96, 1395-1400.

Nagata, H., Shimoda, S., and Sudo, T. (1974) On dehydration of bound water of sepiolite, Clays and Clay Minerals, 22, 285-293.

505 Ovarlez, S., Giullieri, F., Chaze, A-M., Delamare, F., Raya, J., and Hirschinger, J. (2009)
506 The incorporation of indigo molecules in sepiolite tunnels. Chemistry, a European
507 Journal, 15, 11326-11332.
508
509 Post, J.E., Bish, D.L., and Heaney, P.J. (2007) Synchrotron powder X-ray diffraction
510 study of the structure and dehydration behavior of sepiolite. American Mineralogist, 92,
511 91-97.
512
513 Post, J.E. and Heaney, P.J. (2008) Synchrotron powder X-ray diffraction study of the
514 structure and dehydration behavior of palygorskite. American Mineralogist, 93, 667-675.
515
516 Preisinger, A. (1963) Sepiolite and related compounds: Its stability and application. Clays
517 and Clay Minerals, 10, 365-371.
518
519 Prost, R. (1975) Etude de l' hydratation des argiles: interactions eau-minéral et
520 mécanisme de la rétention de l' eau. PhD Thesis, Université Paris VI, (1975)
521
522 Ruiz-Hitzky, E. (2001) Molecular access to intracrystalline tunnels of sepiolite. Journal
523 of Materials Chemistry, 11, 86-91.
524
525 Ruiz-Hitzky, E., Darder, M., Fernandes, F.M., Wicklein, B., Alcântara, A.C.S., and
526 Aranda, P. (2013) Fibrous clays based bionanocomposites. Progress in Polymer Science,
527 38, 1392-1414.

Sánchez del Rio, M., García-Romero, E., Suárez, M., Da Silva, I., Fuentes-Montero, L., and Martínez-Criado, G. (2011) Variability in sepiolite: Diffraction studies, American Mineralogist, 96, 1443-1454.

Serna, C., Ahlrichs, J.L., and Serratosa, J.M. (1975) Folding in sepiolite crystals, Clays and Clay Minerals, 23, 452-457.

Stathopoulou, E.T., Suárez, M., García-Romero, E., Sánchez del Río, M., Kacandes, G.H., Gionis, V., and Chryssikos G.D. (2011) Trioctahedral entities in palygorskite: Near-infrared evidence for sepiolite-palygorskite polysomatism. European Journal of Mineralogy, 23, 567-576.

Suárez, M., and García-Romero, E. (2013) Sepiolite-palygorskite: A continuous polysomatic series. Clays and Clay Minerals, 61, 461-472.

Suzuki, Y., Tenma, Y., Nishioka, Y., and Kawamata, J. (2012) Chemistry, an Asian Journal, 7, 1170-1179.

Tsiantos, C., Tsampodimou, M., Kacandes, G.H., Sánchez del Río, M., Gionis, V., and Chryssikos, G.D. (2012) Vibrational investigation of indigo-palygorskite association(s) in synthetic Maya blue. Journal of Materials Science, 47, 3415-3428.

551 Valentin, J.L., López-Manchado, M.A., Rodríguez, A., Posadas, P., and Ibarra, L. (2007)
552 Novel anhydrous unfolded structure by heating of acid-pretreated sepiolite. Applied Clay
553 Science, 36, 245-255.
554
555 Vincente Rodriguez, M.A., Lopez Gonzales, J.D., Bañares Muñoz, M.A., and Casado
556 Linarejos, J. (1995) Acid activation of a Spanish sepiolite: II. Consideration of kinetics
557 and physicochemical modifications generated. Clay Minerals, 30, 315-323.
558

559 Figure Captions

560

561 Figure 1. Detail of a sepiolite elementary particle (lath) cross section in the dry (A) and
562 folded (B) states, adapted from Post et al. (2007). The discontinuous octahedral sheet is
563 terminated by two and one OH_2 species per Mg, respectively.

564

565 Figure 2. Ambient ATR (upper) and NIR (lower) absorbance spectra of sepiolite SepSp-
566 1 subjected to heating at 175 and 375 °C. The spectra are off set for clarity.

567

568 Figure 3. Ambient 2nd derivative spectra of sepiolite SepSp-1subjected to heating at 175
569 and 375 °C over selected mid- and near-infrared ranges.

570

571 Figure 4. Dependence of OH stretching overtone and H_2O combination modes of
572 sepiolite SepSp-1 on temperature. The shading intensity scales with the amplitude of the
573 2nd derivative signal (as in Fig 3) and the size of the points is proportional to its width
574 between zero-crossings.

575

576 Figure 5. Thermogravimetric analysis data (d*wt*%/d*T*) of sepiolite SepSp-1 (upper) and
577 CAB (lower) as a function of heating rate *q*. In order of increasing temperature, the three
578 weight loss events are due to surface/zeolitic dehydration and removal of the 1st and 2nd
579 Mg-coordinated OH_2. Points ($1/T$,$-\ln q/T_{max}^2$) are used for the calculation of E_a according
580 to Kissinger et al. (2000). Straight lines are least square fits and exclude the lowest *T* -
581 highest *q* points.

582

583 Figure 6. Dynamic heating rate DTG curves of the folding dehydration event in sepiolite
584 SepSp-1 and CAB. Heating rate is ~ 0.2 °C/min.

585

586 Figure 7. Ambient NIR absorbance spectra of sepiolite SepSp-1 leached with 2M H_2SO_4
587 for 1h and subjected to heating at 175 and 375 °C. The spectra are off set for clarity. The
588 y-axis scale is the same as in Fig.2.

589

590 Figure 8. Dependence of the OH stretching overtone modes of acid activated sepiolite
591 SepSp-1 (2M H_2SO_4, 1h) on temperature. Points are defined as in Fig. 4 with the only
592 difference that the darkest shading here corresponds to a smaller maximum intensity
593 (55% of that in Fig. 4).

594

595 Figure 9. The tunnel *ab* plane structure of partially OH_2 dehydrated but unfolded
596 sepiolite is depicted as a fivefold coordinated Mg^{2+} (star), assumed to be labile along the
597 *c* axis. Compare with Fig. 1a. For details see text.

Table 1. Characteristic infrared band positions (cm^{-1}) of folded sepiolite SepSp-1 and their assignment.

ν (cm^{-1})	**assignment**	**ν (cm^{-1})**	**assignment**
7307	ν_{02} SiO-H, X=87 cm^{-1}	3740	ν_{01} SiO-H *
7283	(ν_{02}) SiO-H, X=84 cm^{-1}	3725	ν_{01} SiO-H *
7264	ν_{02} SiO-H, X=85 cm^{-1}	3719	ν_{01} SiO-H
7218	ν'_{02} Mg_3O-H, X=83 cm^{-1}	3692	ν'_{01} Mg_3O-H
7181	ν_{02} Mg_3O-H, X=84 cm^{-1}	3674	ν_{01} Mg_3O-H
6980	ν'_{02} OH_2, X=111 cm^{-1}	3601	ν'_{01} OH_2
6915	ν_{02} OH_2, X=75 cm^{-1}	3532	ν_{01} OH_2
6750	(ν'_{01}+2δ) OH_2	1613	δ OH_2
6690	(ν_{01}+2δ) OH_2	1150	ν Si-O-Si inter-ribbon
5191	(ν'_{01}+δ) OH_2,	1100-900	ν tetrahedral sheet
5122	(ν_{01}+δ) OH_2		
4569	(ν_{01}+δ) SiOH	864	δ SiOH (?)
4544	(ν_{01}+δ) SiOH		
4327	(ν_{01}+δ) Mg_3OH	657	δ Mg_3OH
4310	(ν_{01}+δ) Mg_3OH		

* These bands disappear upon exposure to ambient

a.

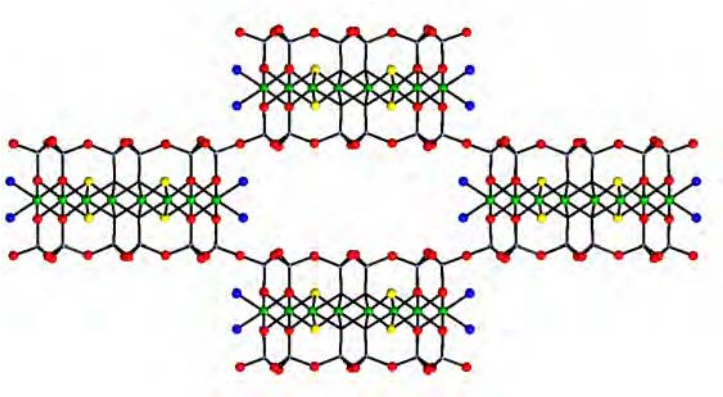

b.

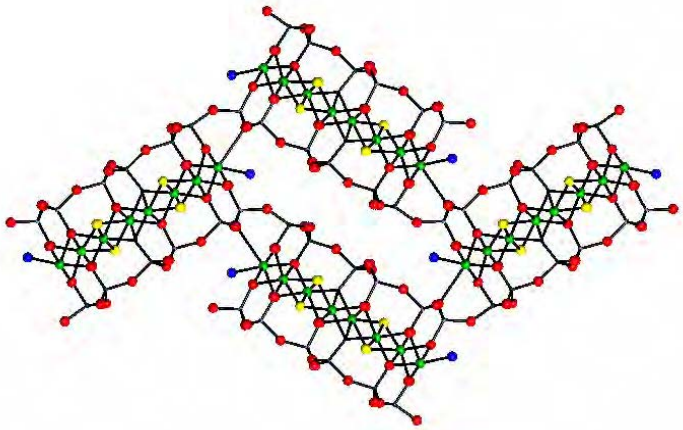

Tsampodimou et al. Fig. 1

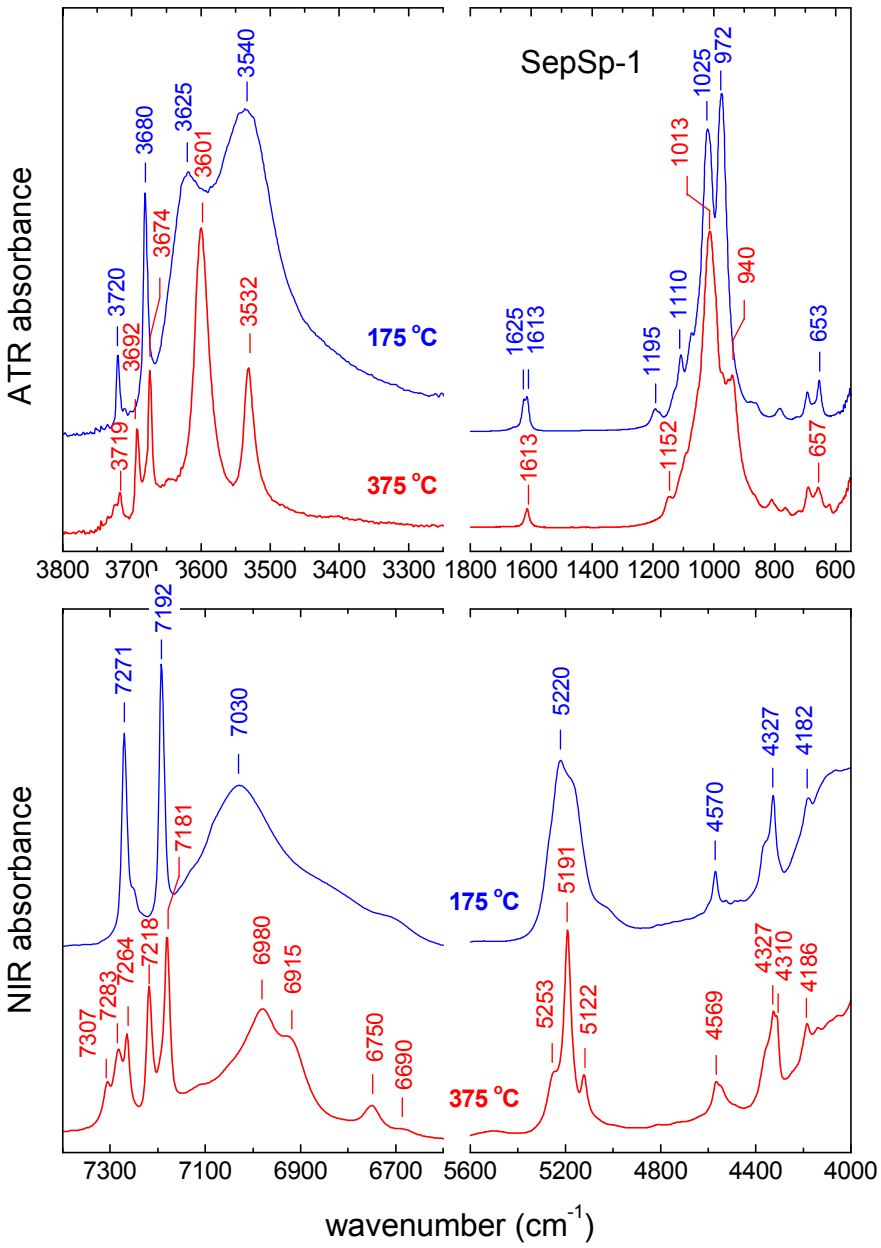

Tsampodimou et al. Fig. 2

This is a preprint, the final version is subject to change, of the American Mineralogist (MSA)
Cite as Authors (Year) Title. American Mineralogist, in press.
(DOI will not work until issue is live.) DOI: http://dx.doi.org/10.2138/am-2015-4988

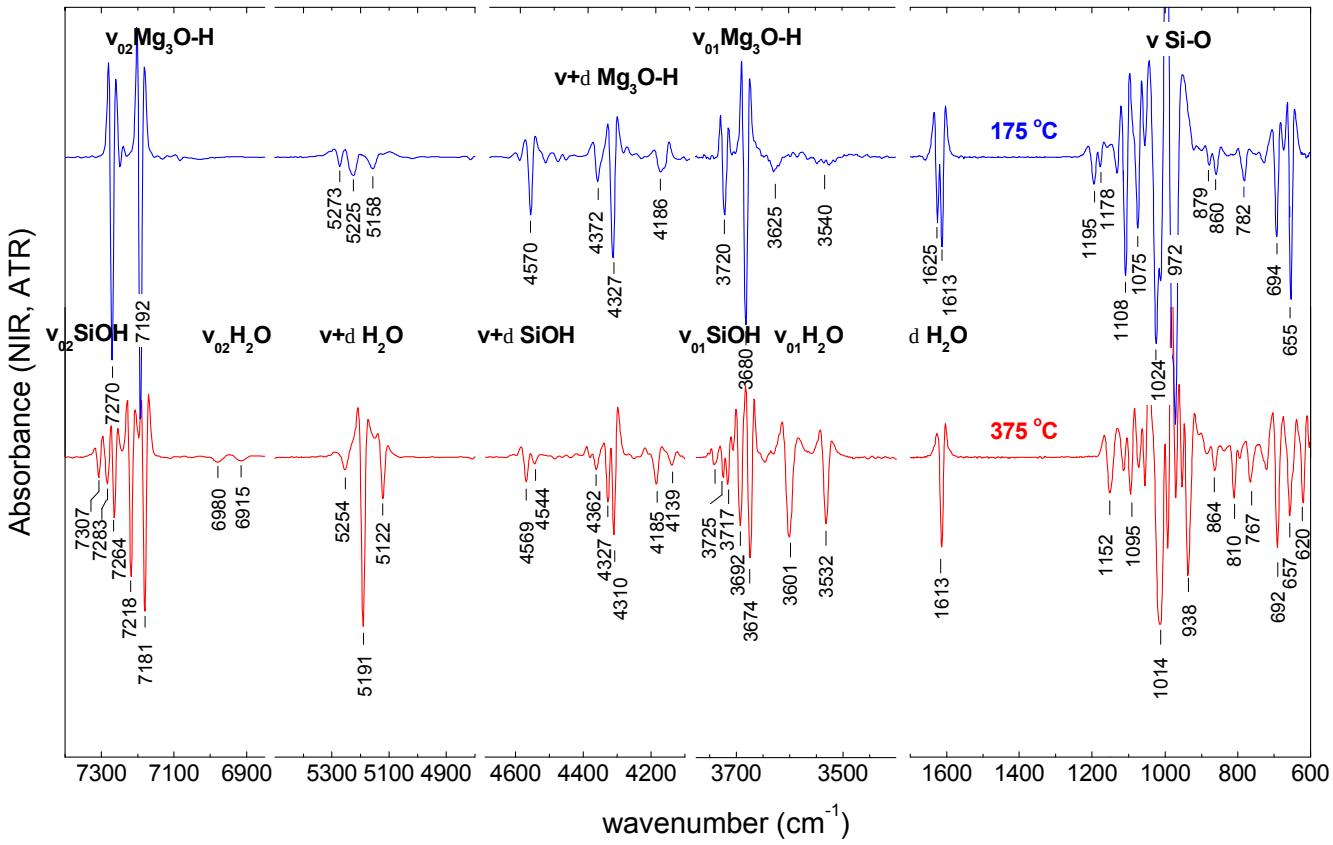

Tsampodimou et al. Fig. 3

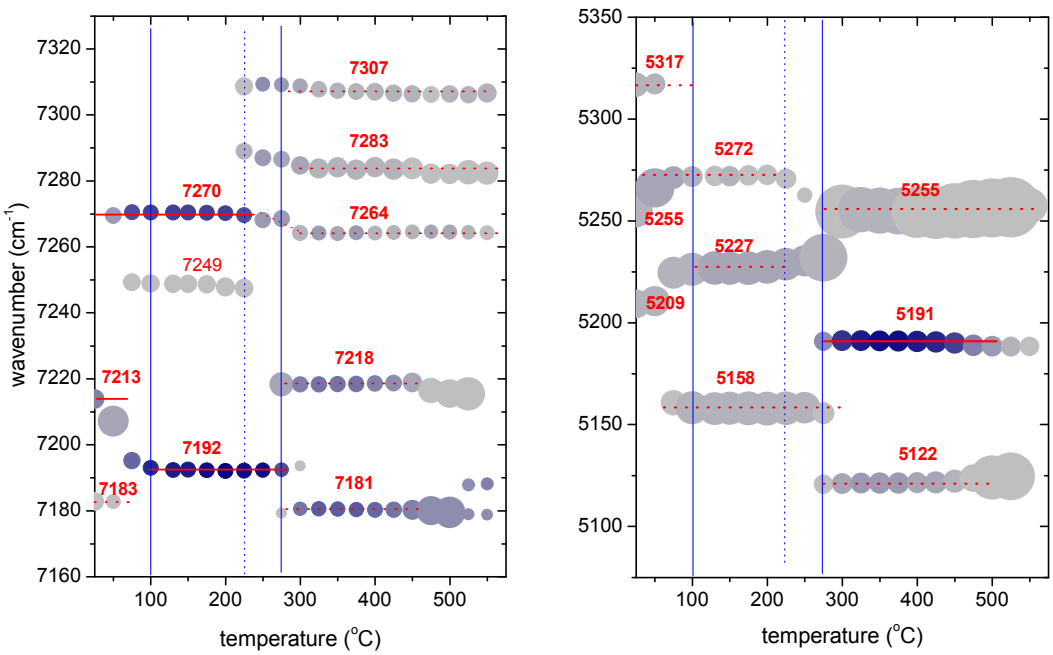

Tsampodimou et al. Fig. 4

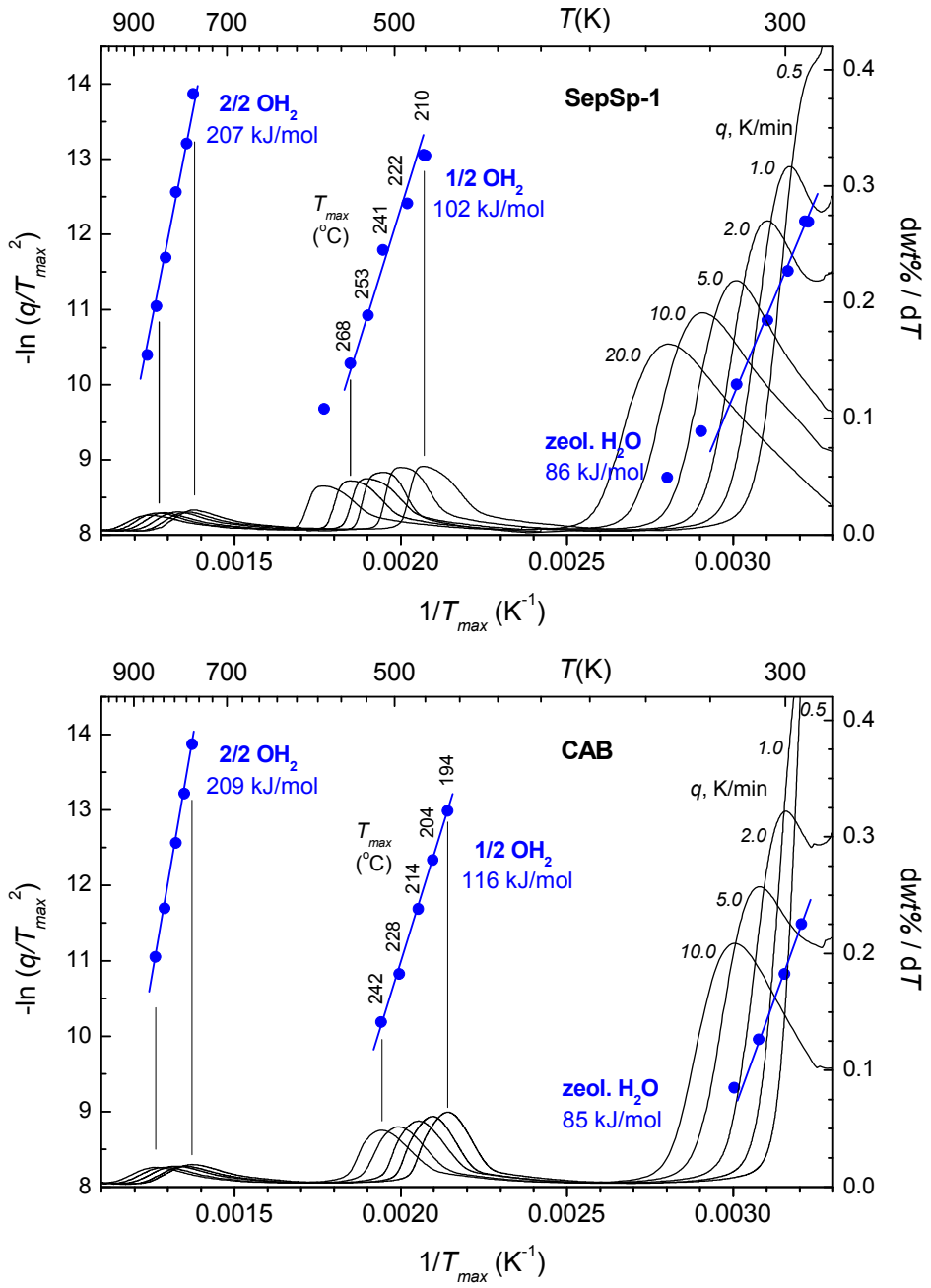

Tsampodimou et al. Fig. 5 R1

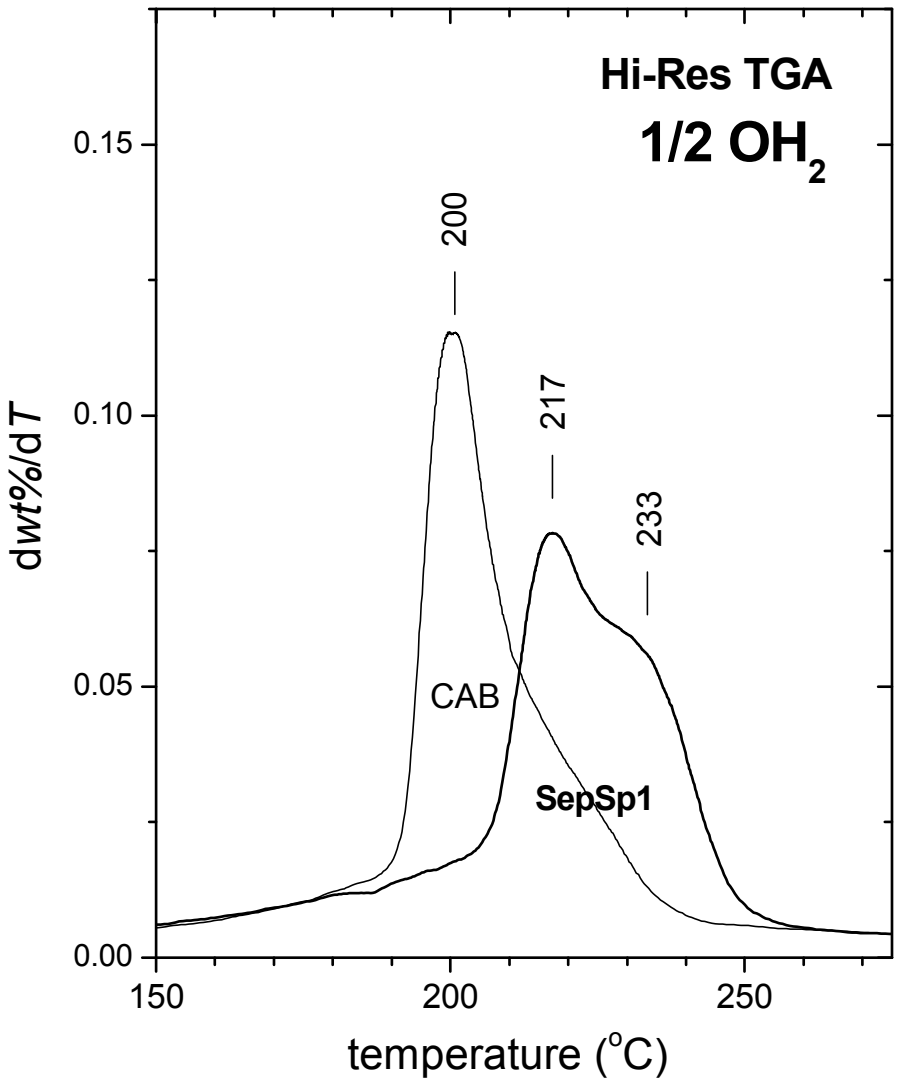

Tsampodimou et al. Fig. 6R1

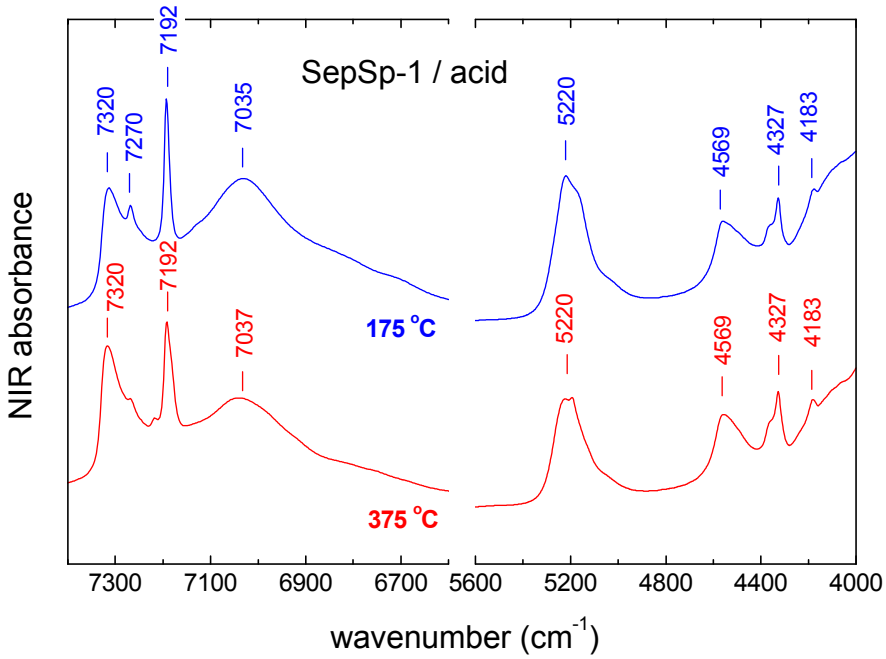

Tsampodimou et al. Fig. 7

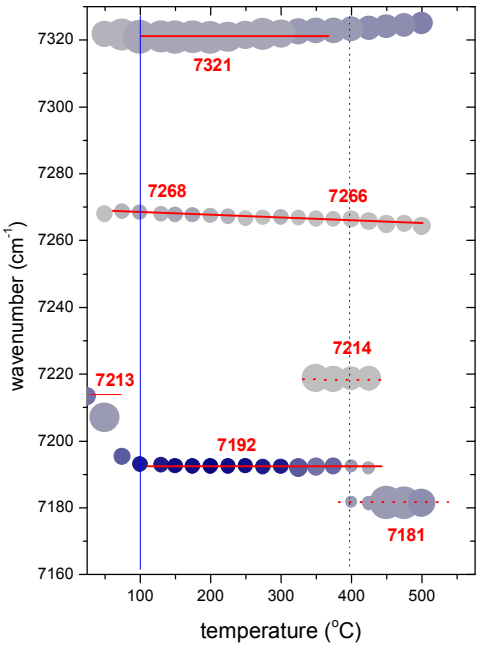

Tsampodimou et al. Fig. 8

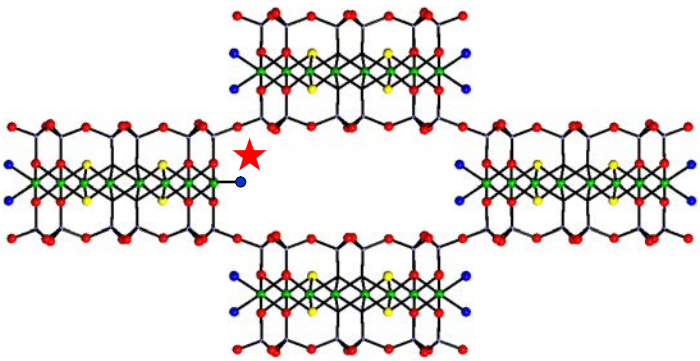

Tsampodimou et al. Fig. 9